Backward $\pi^- d$ elastic scattering from 496 to 1050 MeV/c *

R. Keller,† D. G. Crabb,‡ J. R. O'Fallon, and T. J. Richards§
Physics Department, Saint Louis University, St. Louis, Missouri 63103

L. S. Schroeder
Institute for Atomic Research and Department of Physics, Iowa State University, Ames, Iowa 50010

R. J. Ott,‖ J. Trischuk, and J. Va'vra**
Physics Department, McGill University, Montreal, Canada
(Received 23 December 1974)

Measurements of the differential cross sections for $\pi^- d$ elastic scattering in the backward angular region are presented. These measurements were made at thirteen incident-pion momenta ranging from 496 to 1050 MeV/c, over the center-of-mass angular range 148° to 177°. The experiment was performed at the LBL Bevatron. Experimental apparatus consisted of a liquid deuterium target and a double-arm spectrometer which included scintillation-counter hodoscopes. Center-of-mass differential cross sections were found to be generally smooth over the angular range covered and can be fitted with low-order polynomials. The extrapolated differential cross sections at 180° scattering angle were found to decrease rapidly with increasing momentum, with a prominent peak near 700 MeV/c and a shoulder near 900 MeV/c. These data are discussed in terms of existing models employing "d^*" structures, and are compared with other similar measurements.

I. INTRODUCTION

A counter experiment to measure $\pi^- d$ elastic differential cross sections near 180° has been performed at the Bevatron of Lawrence Berkeley Laboratory. The measurements were made at thirteen momenta in the range of 496 to 1050 MeV/c at approximately 50-MeV/c intervals. The c.m. angular range was from 148° to 177°, with a maximum of eight points per momentum. Preliminary results have been published.[1]

A number of experiments using both bubble-chamber and counter techniques have measured $\pi^- d$ elastic scattering cross sections.[2,3] These experiments concentrated on the forward direction, where it was possible to test theoretical predictions, and thus almost no data were available in the backward direction. The objective of this experiment was to provide a systematic set of measurements of $\pi^- d$ elastic scattering near 180°, where no data previously existed, and to encourage development of multiple-scattering models for large angles. Also, this experiment was intended to allow for a search of $B=2$ resonant states.

The motivation to perform this experiment was provided by the status of the theoretical description of backward hadron-deuteron scattering. Glauber theory[4] with the inclusion of the D-state contribution to the deuteron wave function gives a reasonable representation of froward $\pi^- d$ elastic scattering over a wide range of energies,[3] even at energies where πN resonances occur. However, in regions of strong πN resonances theoretical predictions of total $\pi^- d$ cross sections do not agree well with experiment.[5] Attempts have been made to modify this theory for large-angle scattering by including inelastic contributions,[6,7] higher orders of multiple scattering,[8] more accurate descriptions of the πN amplitudes by using phase-shift solutions,[7] and modifications of the deuteron wave functions to include some type of d^* component. It has been suggested by several authors[9] that such a component could have an N^*N structure. A direct-channel scattering process might include a resonant state with $I=1$, $B=2$. Hence, information on backward $\pi^- d$ elastic scattering could provide evidence for such states, as in the analogous case of $\pi^- p$ elastic scattering in the backward region, which is known to be sensitive to N^* resonances.

The $\pi^- d$ elastic scattering differential cross sections are presented numerically and graphically in Sec. IV. The data are also discussed in view of other existing and related experiments.

II. EXPERIMENTAL PROCEDURE

The experimental method used in this experiment was basically the same as that for a $\pi^- p$ experiment described in a previous article.[10] The same incident pion beam was used with the cryogenic target filled with liquid deuterium (LD_2). To reduce energy loss and multiple Coulomb scattering a short target of 10.6 cm was used when the beam momentum was less than 650 MeV/c. A target of 21.1 cm length was used for higher momenta. Finally, timing changes were made in

the electronic logic for detection of the slower recoil deuterons.

A. Detection system

The particle detection system consisted of a double-arm spectrometer which measured angle-angle correlations between the scattered particles in conjunction with appropriate time-of-flight requirements for elastic scattering. The system is shown schematically in Fig. 1. Scintillation counters S_1, S_2, and S_3 defined the incident pion beam, which was focused on the LD_2 target. Scintillation counter arrays A, B, and C detected the scattered particles. The A array, which consisted of eight counters, detected the back-scattered pions and defined their horizontal angular acceptance. The forward-scattered deuterons were roughly momentum-analyzed and swept away from the forward pion beam by the dipole magnet M_3 and detected in the B and C arrays. The deuteron scattering angle was defined by the fourteen elements of the B counter array. For each counter in the B array there existed a corresponding C counter, which was overmatched to allow for Coulomb scattering and a finite target size. Each pair of BC counters formed a two-counter telescope which defined the scattering region of the forward particles accepted by the system. The G, P, and D counters were extra trigger elements; G defined the vertical acceptance of the system, and the pulse heights from P and D were used to aid in discriminating between protons and deuterons. Elastic events were defined by (i) a beam particle, $S_1S_2S_3$, (ii) a back-scattered particle in fast coincidence (short resolving time), GA_i ($i=1$ to 8), and (iii) a forward, positively charged particle in slow coincidence (long resolving time), PD. The coincidence of these three elements formed a trigger which strobed the B and C arrays. An event was recorded if a particle traversed a matched BC pair with the right time of flight and was in fast coincidence (resolution 20–30 nsec) with the trigger strobe.

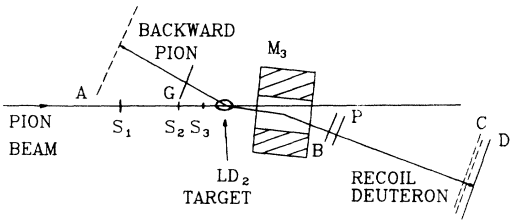

FIG. 1. The particle detection system (not to scale). S_1, S_2, and S_3 are the incident-pion beam counters. The counter hodoscope A and the counter G define the pion backward-scattering region. B and C are counter hodoscopes which detect the recoil particles after passing through the dipole magnet M_3. P and D are additional trigger counters.

B. Proton-deuteron discrimination

The electronic logic used in the $\pi^- p$ experiment[10] was modified to detect the slower recoil deuterons and to discriminate between deuterons and protons produced in the breakup of deuterons. This was achieved by adding an extra arm to the logic which established conditions on time of flight and pulse height from the P and D counters for detection and identification of deuterons (here the letters P and D are to be associated only with the counters and not with protons and deuterons). The logic is shown in Fig. 2. Each pulse from the P and D counters was analyzed by differential discriminators. If the pulse height was greater than a preset discriminator level, $E+\Delta E$, it was identified as a deuteron and the proton identifying coincidence vetoed. If the pulse height fell within the window ΔE, the particle was identified as a proton. To generate a deuteron strobe the particle had to be identified as a deuteron by both the P and D counters. Similarly, to generate a proton strobe the particle had to be identified as a proton by both the P and D counters. The E and ΔE levels for each counter were set from pulse-height discrimination calibrations (see Fig. 3).

Correct time of flight was a further requirement used to identify a particle as a proton or a deuteron. The time delay between the B strobe and the C strobe was set equal to the flight time for deuterons between the B and C counter arrays. This time delay was adjusted through proper delays for each momentum. Hence, if a particle had been identified as a deuteron from its pulse

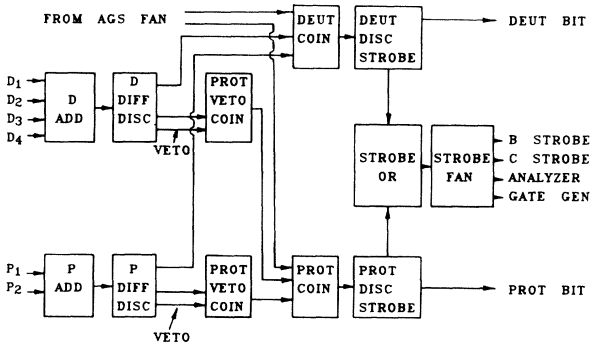

FIG. 2. Proton-deuteron discrimination logic. The differential discriminators analyze the pulse heights of the P and D counters and trigger either a proton or a deuteron strobe. Key: DISC—discriminator, COIN—coincidence, FAN—fanout, DIFF DISC—differential discriminator, GEN—generator.

height, a deuteron strobe was generated which pulsed the B and C arrays at the appropriate times determined from the deuteron time of flight.

The proton rejection efficiency varied with momentum. At momenta less than 800 MeV/c the time-of-flight requirement provided sufficient rejection, and hence the P counter was physically removed from the system to reduce multiple scattering of the deuterons. This rejection efficiency was determined by filling the target with liquid hydrogen and taking a spectrum with the logic system set to accept protons; i.e., both P and D discriminators were adjusted such that every recoil particle was identified as a proton. Further spectra were then taken with the system set to accept deuterons to see how many protons were recorded. Below 800 MeV/c the percentage of protons still recorded (hence unrejected) was less than 0.01%, while above 800 MeV/c and with the P counter in the system it became as high as approximately 0.3%. Since the number of protons produced from deuteron breakup was very large compared to the elastically scattered deuterons, even such a small fraction was significant enough to considerably contaminate the deuteron spectrum at the higher momenta.

The deuteron and proton spectra were stored separately by directly addressing the memory of an ND-2200 pulse-height analyzer as discussed in Ref. 10. The proton spectra were used as a check and a monitor of the proton rejection efficiency.

III. DATA ANALYSIS

The center-of-mass differential cross sections were calculated from

$$\frac{d\sigma}{d\Omega} = \frac{CE}{N_\pi N_d \Delta\Omega} ,$$

where N_π is the number of incident pions, N_d is the number of deuterons per cm^2 in the LD_2 target, $\Delta\Omega$ is the subtended c.m. solid angle, E is the number of elastic scattering events, and C is a correction factor which takes into account deuteron and pion nuclear absorption, multiple scattering, and pion decay.

A. Beam flux and target density

The number of incident pions was determined by subtracting from the number of $S_1S_2S_3$ coincidences the number of leptons contaminating the beam. The beam contamination measurements were made with a threshold gas Cherenkov counter. The fraction of pions in the beam is shown and discussed in the previous article describing the $\pi^- p$ experiment.[10]

The number of deuterons N_d in the target was calculated from the formula

$$N_d = \frac{\rho L N_0}{A} ,$$

where ρ is the density of the liquid deuterium (g/cm^3), L is the effective flask length (cm), N_0 is Avogadro's number (mole^{-1}), and A is the atomic weight (g/mole). The liquid deuterium in the target was filled from a large reservoir and was in thermal equilibrium with it. The vapor pressure was monitored before and after each data-taking run. The density fluctuations observed were typically ±1%. The value of ρ was 0.165 ± 0.002 g/cm^3, giving $N_d = 5.24\times10^{23}$ cm^{-2} for the 10.6-cm target, and $N_d = 1.04\times10^{24}$ cm^{-2} for the 21.1-cm target, with a ±1% uncertainty.

B. Solid-angle calculation

The center-of-mass solid angles were calculated by a Monte Carlo computer program which selected random values within specified limits for the beam momentum and divergence, the angle of the scattered pion, the point of interaction inside the target, and the multiple Coulomb scattering angle of the pion and the recoil deuteron through the target, air, and subsequent counters. The beam momentum and divergence were distributed according to a Gaussian distribution between upper and lower limits. The interaction point of the pion inside the target volume was weighted with the beam profile. The program also included energy loss in the liquid deuterium target and counters. This computation was carried out to ±3% statistical accuracy. The solid angle was also calculated by numerical integration (not by the Monte Carlo method). The results of the two calculations agreed within ±5%. The solid angle ranged from approximately 3.5×10^{-3} to 9.5×10^{-3} sr.

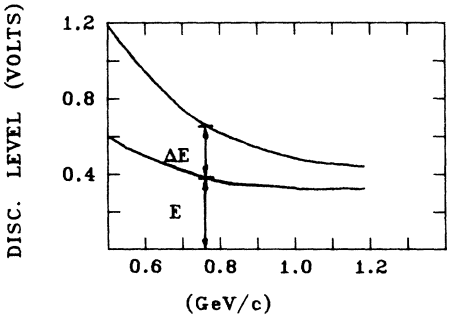

FIG. 3. The curves show the discriminator level setting for counting deuterons and protons. Pusle heights surpassing the $E + \Delta E$ level are counted as deuterons, and pulse heights falling in the ΔE window but above E level are counted as protons.

C. Elastic events, background, and corrections

The number of elastic events was determined from the deuteron spectra similar to that shown in Fig. 4. The locations and widths of the elastically scattered deuteron peaks were in close agreement with the predictions from a Monte Carlo calculation. Each peak had a maximum width of four to five channels because of beam divergence, momentum spread, and multiple scattering in the air, the liquid deuterium target, the target walls, and the counters. The total number of scattering events was obtained by integrating under the peaks.

It was necessary to subtract background events from the total events in order to obtain the number of elastic scattering events. Background events were generated from two main sources: (1) protons from deuteron breakup (called "quasielastic" events) and (2) target-empty and accidental events.

In order to calculate the number of "quasielastic" protons that could be identified by the logic as elastically scattered deuterons it was necessary to measure their spectrum and then multiply by the measured proton rejection efficiency (with appropriate normalizations) to find the number in the elastic deuteron peak. Quasielastic protons were those that arose from deuteron breakup and created pulse heights in the P and D counters in the range of those caused by deuterons and had the correct time of flight to be accepted by the system as elastic deuterons. This quasielastic spectrum was measured by simply setting the P and D discriminators to identify only protons and consequently strobing only the proton arm of the logic. The quasielastic subtraction accounted for approximately 25% of the total background and was concentrated in a small peak under the elastic deuteron peak. The two peaks were only one to two channels apart.

The remaining 75% of the background was largely beam-rate-associated accidentals. Events obtained from an empty target were less than 1% and hence were neglected. Accidentals were a problem with those A counters which were close to the pion beam and experienced a very high singles counting rate. In turn a number of accidental AGS strobes were generated producing a large broad background in the BC spectra associated with these A counters. The total background was seen to be more or less evenly distributed throughout the deuteron spectrum and could be estimated by fitting a smooth curve through it. The uncertainty of these fits was incorporated in the error bar of each data point. Background events for all data points ranged from approximately 10% at low momentum to 50% of the total events at high momentum.

The possibility of inelastic events being detected as elastic events was also investigated. Inelastic events that consisted of production of more than one charged particle were easily rejected by our logic. Reactions with neutral particles in the final state were a more likely source of contamination. The reaction most likely to occur was $\pi^- d \to d\pi^-\pi^0$. A computer program, FOWL,[11] was used to calculate the final-state phase-space density of this reaction and showed that the number of such events in the region of phase space covered by our experiment was negligible. Inelastic events also tend to produce a broad background rather than the sharp peak expected from elastic scattering.

Corrections were made to the number of events to compensate for pions which decayed between the target and the A array and for nuclear absorption of the pion or the deuteron in the target, the air, and the counters. Pion decay corrections were calculated with a Monte Carlo computer program. Muons from pion decay randomly hit adjoining A counters, which caused the deuteron detected by the BC counters to be associated with the wrong A counter. Hence each A counter would both lose some counts due to pion decay and gain back some counts from pion decay in the angular region of the adjoining A counters. A correction factor F was calculated using

$$F = N_{\text{inc}}/(N_{\text{inc}} - N_{\text{miss}} - N_{\text{out}} + N_{\text{in}}) ,$$

where N_{inc} is the number of pions incident on the A counter and N_{miss} is the number of muons that completely missed the A array. For the A counters on the edges of the array, more muons were

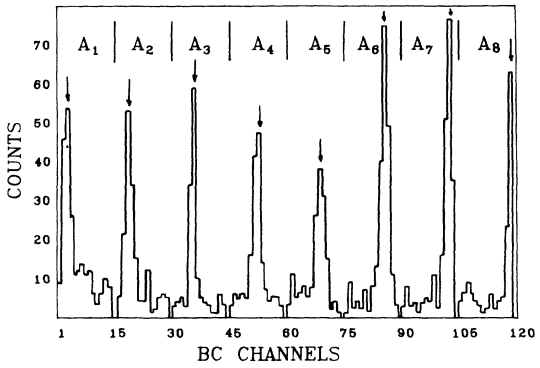

FIG. 4. The deuteron spectrum at 739 MeV/c. A 14-channel BC spectrum is displayed for each of the eight A counters. The elastic peaks can clearly be seen over the broad background. The center of each elastic scattering distribution from Monte Carlo predictions is shown by the arrow.

lost (N_{out}) than were gained (N_{in}) and hence the correction factor F was typically larger (about 1.03) than for A counters near the center of the array (about 1.01). This number was still slightly larger than 1.00 because N_{miss} was never zero even when N_{out} was equal to N_{in}. Equal numbers of muons lost could be compensated by equal numbers of muons gained since the associated shifts in the deuteron spectra were never outside the elastic events peak, which was normally four to five BC channels wide.

The nuclear absorption correction was larger and varied between $(24 \pm 5)\%$ and $(32 \pm 5)\%$, hence presenting the major correction to be made to the data. Pions and deuterons could be absorbed in the deuterium target, the target vessel and insulation, the vacuum chamber window, the air, and the plastic scintillation counters. The correction factors were calculated by using the total cross section minus the forward elastic scattering cross sections for pion and deuteron scattering on these materials. In this momentum range the only deuteron total cross section data available were for the dd reaction.[12] The correction for deuteron absorption in other materials was estimated by calculating an equivalent amount of deuterium and using the dd total cross sections.

IV. RESULTS

The results of this experiment are displayed graphically in Fig. 5 and are tabulated in Table I. The errors shown are a combination of a statistical error and a point-to-point error due to background subtraction. In addition there were systematic errors, which included (1) $\pm 3\%$ for the solid-angle uncertainty, (2) $\pm 2\%$ uncertainty in beam contamination, (3) $\pm 1\%$ uncertainty in target volume and density determination, (4) $\pm 5\%$ uncertainty in the absorption correction factors, (5) $\pm 0.5\%$ for the pion-decay correction factors, and (6) $\pm 3\%$ for counter inefficiencies. These uncertainties were added in quadrature to give an over-all systematic error of $\pm 7\%$ to be associated with each data point. The fits shown with the data are functions

$$\sum_{l=0}^{3} a_l P_l(\cos\theta) ,$$

which gave a lower reduced χ^2 than a first- or second-order fit. For some momenta a polynomial with $l_{max} = 2$, however, gave an equally good fit. These fits serve mainly for extrapolation purposes and have no physical significance. For all momenta presented, the data are generally smooth and flat throughout the angular range. At the lower momenta some peaking can be seen in the near backward region, as well for a few momenta near 700 MeV/c. At the higher momenta, the errors become so large that it becomes difficult to make any conclusions about the general trend.

Figure 6 shows the values of the differential cross sections obtained by extrapolating to 180° scattering angle using these polynomial fits and shows significant structure as a function of the laboratory momentum of the incident pion. The plot shows a general exponential decrease with a peak near 700 MeV/c and a shoulder near 900 MeV/c. To ascertain the significance of this structure, a superimposed line is also shown. This line, which was fitted to represent the general slope of the data, has the form $\exp(-0.0066 P_{lab})$. There is a probability of $<10^{-4}$ that such a function will fit the data, and the peak near 700 MeV/c deviates by about 10 standard deviations from it.

The fits to the differential cross sections as a function of scattering angle and momentum are displayed in the three-dimensional plot shown in Fig. 7, and give an over-all view of the data. Some evidence of the structures seen in the 180° cross section at 700 MeV/c and 900 MeV/c persist over the entire angular range covered by this experiment.

V. INTERPRETATIONS AND CONCLUSIONS

Only a qualitative discussion of the data can be given since no adequate theory yet exists which can be directly applied to our data. There are several models in existence that deal with hadron-deuteron elastic scattering, but they have only been able to describe the elastic differential cross section near the forward direction with any degree of success. Pion-deuteron elastic scattering for larger angles must include higher-order multiple-scattering terms, relativistically invariant deuteron form factors, and possibly inelastic intermediate states such as nucleon resonances. These problems have been carefully investigated recently by several authors.[13] However, in spite of an inadequate theory, the data presented here should give some additional insights into the matter, which will be presented in the following discussion.

An application of the multiple-scattering model as was done by Wallace[14] has given a good description to the forward-scattering data of Bradamente *et al.*[15] (seen in Fig. 8), and might be expanded to include our contribution at 901 MeV/c. If higher-order multiple scattering dominates near the backward region, individual πN resonances also become important. Our data near $\cos\theta = -0.88$ extrapolate nicely with the forward scattering data, possibly suggesting a dominant

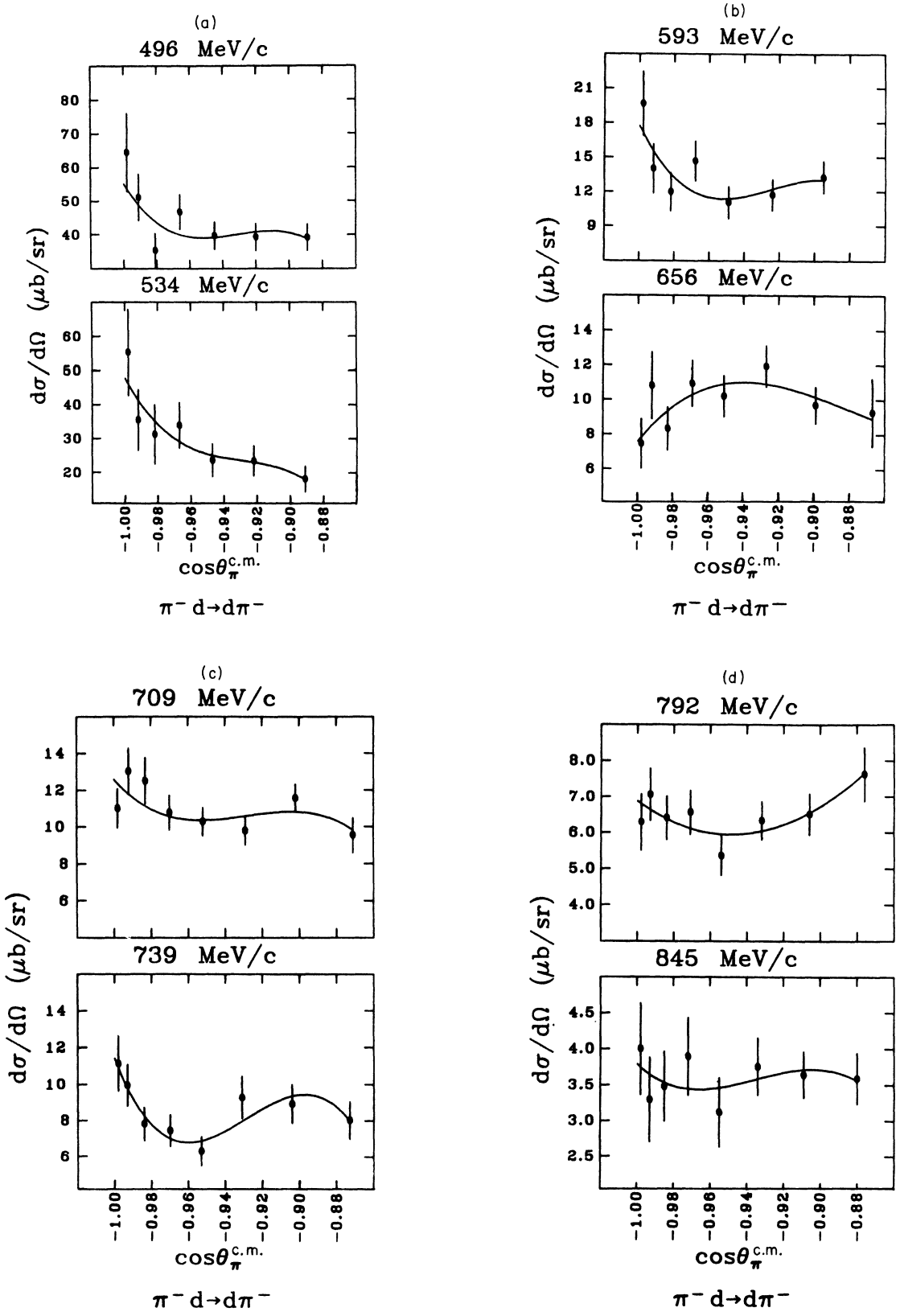

FIG. 5. *(Continued on following page).*

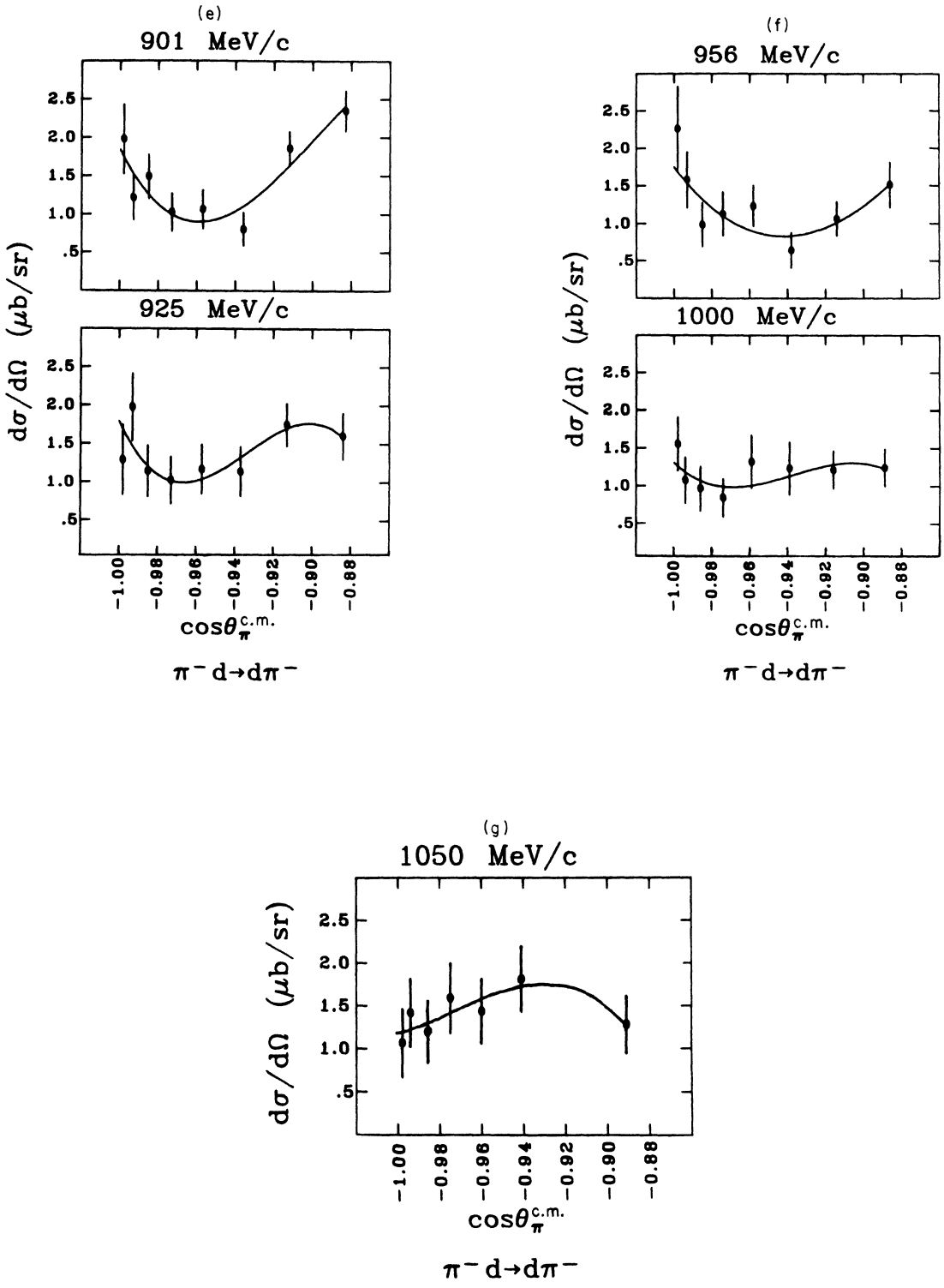

FIG. 5. Differential cross sections for $\pi^- d$ elastic scattering as a function of the c.m. scattering angle. All curves are Legendre polynomial ($l=3$) fits.

TABLE I. $\pi^- d$ elastic differential cross sections in the center-of-mass system.

P_{lab} [a] (MeV/c)	E_{cm} [b] (MeV)	$-\cos\theta_{cm}$	$d\sigma/d\Omega$ (μb/sr)	u [(GeV/c)^2]	$d\sigma/du$ [mb/(GeV/c)^2]	Error [c] (%)	P_{lab} [a] (MeV/c)	E_{cm} [b] (MeV)	$-\cos\theta_{cm}$	$d\sigma/d\Omega$ (μb/sr)	u [(GeV/c)^2]	$d\sigma/du$ [mb/(GeV/c)^2]	Error [c] (%)
496	2339	0.9975	64.3	2.236	1276.8	18	845	2598	0.9980	4.00	1.811	33.8	16
		0.9914	51.1	2.234	1014.7	14			0.9931	3.29	1.808	27.8	18
		0.9811	35.3	2.231	701.0	14			0.9846	3.48	1.801	29.4	14
		0.9658	46.7	2.226	927.3	11			0.9721	3.89	1.792	32.8	14
		0.9453	39.7	2.220	788.3	10			0.9555	3.11	1.780	26.3	16
		0.9196	39.3	2.212	780.4	11			0.9344	3.75	1.764	31.7	11
		0.8889	39.2	2.201	778.4	10			0.9090	3.64	1.745	30.7	9
									0.8798	3.59	1.723	30.3	10
534	2368	0.9976	55.6	2.181	969.5	23							
		0.9917	35.4	2.179	621.7	25	901	2638	0.9981	1.97	1.757	15.1	23
		0.9815	31.2	2.176	548.0	28			0.9933	1.21	1.753	9.3	24
		0.9666	33.9	2.170	595.4	20			0.9850	1.49	1.747	11.4	20
		0.9467	23.6	2.163	414.5	21			0.9730	1.02	1.737	7.8	24
		0.9215	23.4	2.154	411.0	19			0.9568	1.06	1.723	8.1	24
		0.8915	18.1	2.143	317.9	22			0.9368	0.80	1.707	6.1	27
									0.9116	1.85	1.686	14.2	12
593	2413	0.9977	19.6	2.101	289.8	14			0.8832	2.35	1.663	18.0	11
		0.9920	14.0	2.098	207.0	15							
		0.9821	12.0	2.094	177.4	14	925	2654	0.9981	1.29	1.735	9.5	36
		0.9678	14.6	2.088	215.9	12			0.9934	1.97	1.731	14.5	22
		0.9486	11.0	2.080	162.7	13			0.9852	1.34	1.724	9.8	30
		0.9243	11.7	2.070	173.0	12			0.9733	1.02	1.714	7.5	30
		0.8952	13.2	2.057	195.2	11			0.9573	1.17	1.700	8.6	28
									0.9371	1.14	1.683	8.4	29
656	2460	0.9978	7.5	2.020	94.2	19			0.9126	1.75	1.662	12.9	16
		0.9923	10.8	2.018	135.7	18			0.8846	1.60	1.638	11.8	19
		0.9828	8.3	2.013	104.3	15							
		0.9690	10.9	2.006	136.9	12	956	2676	0.9981	2.26	1.707	15.8	25
		0.9505	10.2	1.997	128.1	12			0.9935	1.57	1.703	11.0	24
		0.9271	11.9	1.985	149.5	10			0.9855	0.98	1.696	6.9	30
		0.8990	9.7	1.971	121.9	11			0.9737	1.12	1.685	7.8	26
		0.8669	9.3	1.955	116.8	21			0.9580	1.23	1.671	8.6	22
									0.9380	0.64	1.653	4.5	38
709	2500	0.9978	11.0	1.957	122.1	10			0.9140	1.06	1.631	7.4	22
		0.9925	13.0	1.954	144.3	10			0.8864	1.51	1.607	10.6	20
		0.9834	12.5	1.949	138.8	10							
		0.9700	10.8	1.942	119.9	9	1000	2706	0.9982	1.55	1.669	10.1	23
		0.9520	10.3	1.931	114.3	8			0.9936	1.07	1.664	7.0	29
		0.9293	9.8	1.919	108.8	8			0.9858	0.96	1.657	6.3	31
		0.9020	11.6	1.903	128.8	7			0.9743	0.84	1.646	5.5	31
		0.8708	9.5	1.885	105.5	10			0.9589	1.32	1.631	8.7	27
									0.9394	1.23	1.612	8.0	29
739	2522	0.9979	11.1	1.923	115.4	14			0.9158	1.21	1.590	7.9	21
		0.9926	9.9	1.920	102.9	12			0.8887	1.24	1.564	8.1	20
		0.9836	7.8	1.915	81.1	12							
		0.9704	7.4	1.907	76.9	12	1050	2740	0.9982	1.06	1.627	6.5	38
		0.9528	6.3	1.896	65.5	13			0.9938	1.41	1.623	8.6	29
		0.9305	9.3	1.883	96.7	13			0.9861	1.19	1.615	7.2	31
		0.9037	8.9	1.866	92.5	12			0.9749	1.58	1.603	9.6	26
		0.8729	8.0	1.848	83.2	13			0.9599	1.43	1.588	8.7	27
									0.9408	1.81	1.568	11.0	21
792	2560	0.9979	6.28	1.866	58.6	13			0.8914	1.27	1.517	7.7	27
		0.9929	7.05	1.862	65.8	10							
		0.9841	6.40	1.856	59.7	10							
		0.9713	6.55	1.848	61.1	9							
		0.9542	5.35	1.836	49.9	10							
		0.9325	6.33	1.822	59.1	9							
		0.9064	6.50	1.804	60.7	9							
		0.8795	7.62	1.784	71.1	10							

[a] Laboratory momentum of the incident beam.

[b] Total energy in the c.m. system.

[c] The errors quoted are a combination of statistical error and point-to-point error due to background subtraction corresponding to one standard deviation.

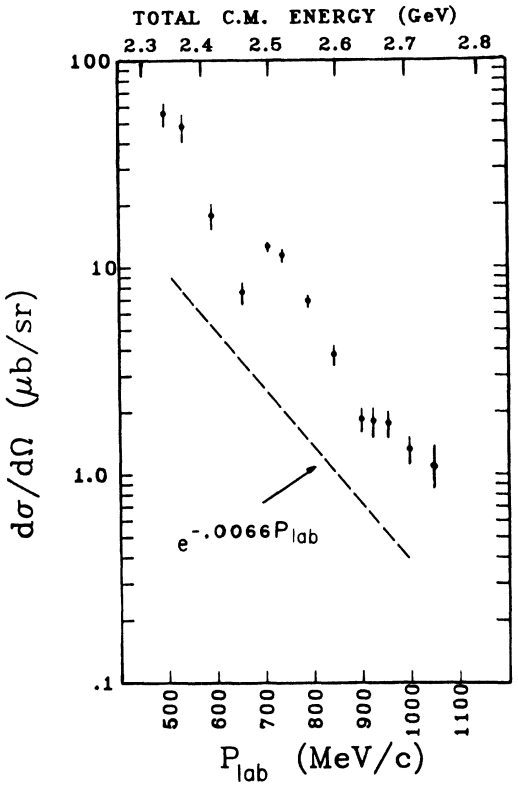

FIG. 6. Differential cross sections for $\pi^- d$ elastic scattering at 180° c.m. scattering angle as a function of laboratory momentum of the incident pion. These are extrapolated values using the polynomial fits seen in Fig. 5. The dashed curve is an arbitrary line with a slope obtained from a fit of the data.

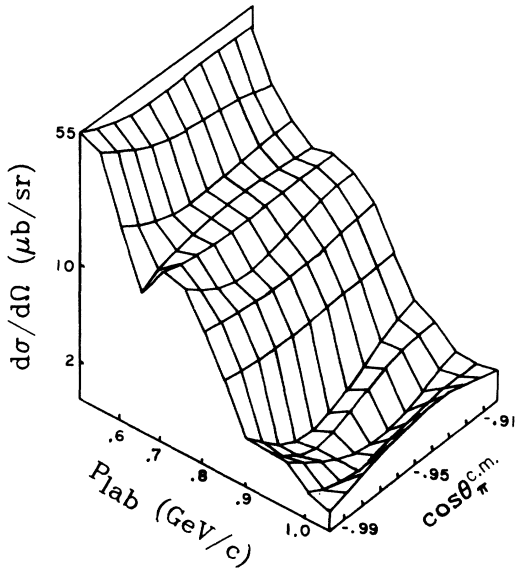

FIG. 7. Three-dimensional plot of the elastic $\pi^- d$ scattering data, showing only the polynomial fits of Fig. 5.

double-scattering term. At larger angles up to $\cos\theta = -1.0$, our data show a significant dip and a steep rise near $\cos\theta = -1.0$, which may show some dominant higher-order multiple-scattering or πN-resonance contribution.

Kerman and Kisslinger[9] suggested that an $N^* N$ component with proper quantum numbers should be included in the deuteron wave function. Such a contribution is expected to be about 1% or more

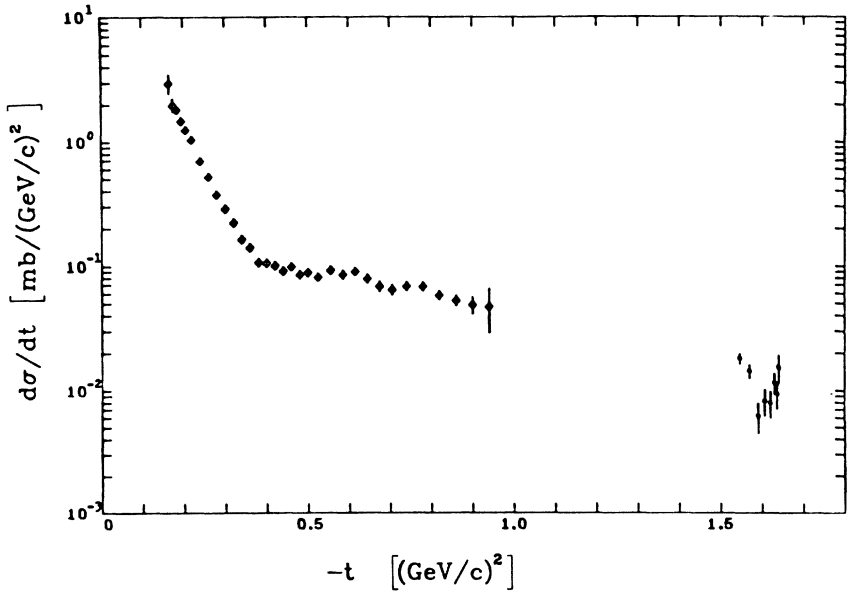

FIG. 8. Forward $\pi^- d$ elastic scattering data of Bradamente *et al.*, Ref. 15 (◆) at 895 MeV/c with our data at 901 MeV/c (●).

of the wave function, and could dominate the backward scattering region, as Kerman and Kisslinger have shown for the pd elastic scattering process. The rise in the backward $\pi^- d$ elastic differential cross section seen in our data could be the result of such N^*N contribution. The structures near 700 and 900 MeV/c seen in our data are best explained by the D'_{13} and F'_{15} nucleon resonances as shown in Table II.

Experiments by Carter *et al.*[16] (measurements of $\pi^- d$ total cross sections) and Armstrong *et al.*[17] (measurements of γd total cross sections) also show results that support the notions of an N^*N model. Their experiments show enhancements in the deuteron total cross section at the same c.m. energies as in our experiment. Further, these authors also established from their respective $\pi^- p$ and γp total scattering cross-section data N^* resonances that had masses equal to the N^*N-N mass. Among these were the well-known D'_{13} and F'_{15} resonances. They also observed the width of the N^*N configuration to be generally broader than the corresponding N^* resonance, which they interpreted as being a possible result of internal motion of the nucleons in their bound state. Thus, the observed enhancement in the total deuteron cross sections, as measured by these authors, may be the result of nucleon resonance in the bound state with another nucleon.

TABLE II. Resonance parameters.

	Mass (MeV)	N^*N mass (MeV)	Observed structure $\pi^- d$ c.m. energy (MeV)
D'_{13}	1520	2458	2520
F'_{15}	1688	2627	2670

In conclusion, the structures in our $\pi^- d$ elastic-scattering data could be explained in terms of a multiple-scattering model as well as a result of a contribution of a N^*N component in the deuteron wave function. It is hoped that these data will encourage further developments of this model. Alternate interpretations might include a direct-channel model that requires $I=1$, $B=2$ resonances near 2520 and 2570 MeV having low spin so that the angular distributions would remain smooth. However, a theoretical investigation of this model is still nonexistent.

ACKNOWLEDGMENTS

We wish to express our thanks to the Bevatron operating crew and staff for their assistance, as well to Ed McLaughlin and the target group staff for our target. In addition we thank Dr. T. Elioff and Dr. R. Sah for helpful discussions concerning our beam line.

*Work supported in part by the Ames Laboratory of the U. S. Atomic Energy Commission and the National Research Council of Canada.

†Present address: Department of Physics, Brookhaven National Laboratory, Upton, New York 11973.

‡Present address: Nuclear Physics Laboratory, Oxford University, Oxford, England.

§Present address: Research Department, Caterpillar Tractor Company, Peoria, Illinois 61602.

‖Present address: Lawrence Berkeley Laboratory, Berkeley, California 94720.

¶Present address: Rutherford Laboratory, Chilton, Didcot, Berkshire, England.

**Present address: TRIUMF, University of British Columbia, Vancouver, British Columbia, Canada.

[1]L. S. Schroeder, D. G. Crabb, R. Keller, J. R. O'Fallon, T. J. Richards, R. J. Ott, J. Trischuk, and J. Va'vra, Phys. Rev. Lett. 27, 1813 (1971).

[2]E. G. Pewitt, T. H. Fields, G. B. Yodh, L. G. Fetkovich, and M. Derrick, Phys. Rev. 131, 1826 (1963); H. C. Hsiung, E. Coleman, B. Roe, D. Sinclair, and J. Van der Velde, Phys. Rev. Lett. 21, 187 (1968).

[3]F. Bradamente, S. Conelli, G. Fidecaro, M. Fidecaro, M. Giorgi, A. Penzo, L. Piemontese, F. Sauli, P. Schiavon, and A. Vascotto, Phys. Lett. 28B, 193 (1968); M. Fellinger, E. Gutman, R. C. Lamb, F. C. Peterson, L. S. Schroeder, R. C. Chase, E. Coleman, and T. G. Rhoades, Phys. Rev. Lett. 22, 1265 (1969); F. Bradamente, G. Fidecaro, M. Fidecaro, M. Giorgi, P. Palazzi, A. Penzo, L. Piemontese, F. Sauli, P. Schiavon, and A. Vascotto, Phys. Lett. 31B, 87 (1970).

[4]R. J. Glauber, in *Lectures in Theoretical Physics*, edited by W. E. Brittin *et al.* (Interscience, New York, 1959), Vol. 1; R. J. Glauber, Phys. Rev. 100, 242 (1955).

[5]G. Fäldt and T. E. O. Erickson, Nucl. Phys. B8, 1 (1968).

[6]D. R. Harrington, Phys. Rev. 184, 1745 (1969); Carl Carlson, Phys. Rev. C 2, 1224 (1970).

[7]G. Albieri and L. Bertocchi, Nuovo Cimento 61A, 203 (1969).

[8]J. Pumplin, Phys. Rev. 173, 1651 (1968).

[9]A. K. Kerman and L. S. Kisslinger, Phys. Rev. 180, 1483 (1969); N. R. Nath, H. J. Weber, and P. K. Kabir, Phys. Rev. Lett. 26, 1404 (1971).

[10]T. J. Richards, D. G. Crabb, R. Keller, J. R. O'Fallon, R. J. Ott, J. Trischuk, J. Va'vra, and L. S. Schroeder, Phys. Rev. D 10, 45 (1974).

[11]F. James, CERN Computer Library Report No. W505, 1968 (unpublished).

[12]A. T. Goslow, P. J. Oddone, M. J. Basin, and C. R. Inn, Phys. Rev. Lett. 23, 990 (1969).

[13]R. H. Landau, Phys. Rev. D 3, 81 (1971); R. A. Rudin, *ibid.* 1, 2557 (1970).

[14]Jon M. Wallace, Phys. Rev. D 5, 1840 (1972).

[15]F. Bradamente, S. Conetti, G. Fidecaro, M. Fidecaro, M. Giorgi, A. Penzo, L. Piemontese, F. Sauli, and P. Sciavon, Phys. Lett. 28B, 191 (1968).
[16]A. Carter, K. Riley, R. Tapper, D. Bugg, R. Gilmore, K. Knight, D. Salter, G. Stafford, E. Wilson, J. Davies, J. Dowell, P. Hattersley, R. J. Homer, and A. O'Dell, Phys. Rev. 168, 1457 (1968).
[17]T. A. Armstrong, W. R. Hogg, G. M. Lewis, A. W. Robertson, G. R. Brookes, A. S. Clough, J. H. Freeland, W. Galbraith, A. F. King, W. R. Rawlinson, N. R. S. Tait, J. C. Thompson, and D. W. Tolfree, Nucl. Phys. B41, 445 (1972); Phys. Rev. D 5, 1640 (1972).